Theory of resonance and threshold effects in the electronic excitation of molecules by electron impact

M. Ohno* and W. Domcke
Theoretische Chemie, Physikalisch-Chemisches Institut, Universität Heidelberg, D-6900 Heidelberg, West Germany
(Received 22 February 1983)

A simple model of electron scattering resonances near electronic excitation thresholds is discussed. The model consists of a single discrete electronic state coupled to several electronic continua. The vibrational dynamics in the resonance state is treated, taking proper account of non-Born-Oppenheimer effects in near-threshold electron-molecule scattering. The effect of long-range potentials is included via the threshold expansion of the partial decay widths of the resonance. The analytic properties of the fixed-nuclei S matrix are analyzed in detail for two special cases (s-wave scattering in the absence of long-range potentials and scattering from a strongly polar target molecule). The dipole potential is shown to lead to a qualitatively new behavior of the trajectories of resonance poles near excitation thresholds. The model yields a qualitative description of the measured excitation function of the $B\,^1\Sigma^+$ state of the CO molecule, where a strong and narrow threshold peak is observed.

I. INTRODUCTION

For at least two decades the existence of electron scattering resonances has been well established in atoms and molecules.[1,2] In molecules, resonances play an important role in various processes involving a transfer of energy from low-energy electrons to the internal nuclear motion and vice versa.[2–5] Shape resonances supported by the centrifugal barrier of the molecular potential are a very common phenomenon in low-energy electron-molecule scattering. The prototypical example is the 2.3-eV shape resonance in e-N_2 scattering.[2] After a considerable theoretical and computational effort over the past decade, vibrational excitation of N_2 via the 2.3-eV resonance is now well understood.[6–12] The situation is less clear for the resonances and threshold peaks observed by Rohr and Linder in polar molecules such as HF, HCl, and HBr.[13,14] Several theoretical explanations have been put forward,[15–19] but there is still no consensus on the basic nature of the phenomenon, although it is generally believed that the long-range dipole potential plays a decisive role. As emphasized in Refs. 19 and 20, resonances near threshold are nontrivially modified by long-range potentials acting on the scattered electron.

In the present work we extend the model of Refs. 19 and 20 to describe resonances near electronic excitation thresholds. The approach is largely phenomenological, aiming at the analysis of the general features of such resonances. The formalism is based on Feshbach's projection-operator approach[21] or Fano's theory of configuration interaction in the continuum,[22] assuming a single discrete electronic state interacting with several electronic continua. The analytic structure of the multichannel S matrix for electron scattering is analyzed, yielding a unified description of core-excited shape resonances and Feshbach resonances near excitation thresholds. The analytic properties of the S matrix near threshold depend on the angular momentum of the scattered electron and the strength of possible long-range potentials. As specific examples, s-wave scattering by short-range potentials and scattering in the presence of a "critical" dipole potential are worked out in detail. Finally, the vibrational dynamics in such core-excited resonances is treated exactly for a simple model problem, yielding excitation functions for electronic plus vibrational excitation by electron impact. The model gives a qualitative explanation of the threshold peaks observed in the excitation functions of several electronic states of the CO molecule.[23]

II. GENERAL THEORY

It is well known that resonances can be described as discrete states embedded in and interacting with a continuum.[21,22,24–28] In the present work we study electron scattering resonances near the electronic excitation threshold of a target molecule. We consider a very general and simple model describing a single resonance coupled to several electronic continua, including the vibrational motion of the target molecule.

More specifically, we consider a discrete (localized) electronic state $|d\rangle$ interacting with n continua $|k^\alpha\rangle$ ($\alpha=1,\ldots,n$). α is the electronic channel index. $|k^1\rangle$ and $|k^\alpha\rangle$ ($\alpha=2,\ldots,n$) are electronic continua associated with the electronic ground state and the lowest $(n-1)$ excited states with excitation energies $E_{\rm ex}^\alpha$, respectively. An appropriate model Hamiltonian can be written as

$$H=H_0+V\,, \tag{2.1}$$

$$H_0=\tilde{H}_0+\sum_\alpha\sum_k |k^\alpha\rangle(E_{\rm ex}^\alpha+\epsilon_k)\langle k^\alpha| + |d\rangle\epsilon_d\langle d|\,, \tag{2.2}$$

$$\tilde{H}_0 = T_N + V_0(R) , \tag{2.3}$$

$$V = \sum_{\alpha} \sum_{k} (| k^{\alpha} \rangle V_{kd}^{\alpha} \langle d | + \text{H.c.}) . \tag{2.4}$$

Here T_N denotes the kinetic energy of vibrational motion and $V_0(R)$ is the electronic potential energy of the target molecule. $\tilde{H}_0$ is thus the vibrational Hamiltonian of the target. For simplicity, we suppress the rotational degrees of freedom and consider only one vibrational degree of freedom. ϵ_d is the energy of the discrete state and is a function of the internuclear distance R. E_{ex}^{α} is the electronic excitation energy of the target molecule (we define $E_{\text{ex}}^{1}=0$). ϵ_k is the energy of a continuum electron and thus independent of R. The interaction V mixes the discrete state $| d \rangle$ with the continua $| k^{\alpha} \rangle$ ($\alpha = 1, \ldots, n$) and converts $| d \rangle$ into a resonance. For simplicity, we assume V_{dk}^{α} to be independent of R, although this restriction can be easily relaxed.[29]

We now introduce the adiabatic or Born-Oppenheimer (BO) approximation for the basis states. We assume that the electronic wave functions of the discrete state and the continuum states

$$\Phi_d(r,R) = \langle r | d \rangle ,$$

$$\Phi_k^{\alpha}(r,R) = \langle r | k^{\alpha} \rangle ,$$

where r denotes the electronic coordinates collectively, depend sufficiently weakly on the internuclear distance such that

$$[T_N, \Phi_d(r,R)]_- = [T_N, \Phi_k^{\alpha}(r,R)]_- = 0 . \tag{2.5}$$

It should be stressed that the BO approximation is not necessarily a good approximation for the resonance wave function obtained by diagonalizing $H - T_N$ for each R, since the degree of mixing of the basis states $| d \rangle$ and $| k^{\alpha} \rangle$ may vary rapidly with internuclear distance. This may happen, in particular, when the discrete state crosses a threshold.

The initial and final asymptotic states are

$$| i \rangle = | k_i^1 \rangle | 0^1 \rangle , \qquad | f \rangle = | k_f^{\alpha} \rangle | v^{\alpha} \rangle . \tag{2.6}$$

Here $| 0^1 \rangle$ and $| v^{\alpha} \rangle$ are the vibrational ground state of the target molecule in its electronic ground state and the vth excited vibrational state of the target molecule in the αth excited electronic state, respectively. k_i and k_f are the initial and final momenta of the scattered electron for $1 \rightarrow \alpha$ electronic and $0 \rightarrow v$ vibrational excitation. Here we have assumed the BO factorization of the electronic and vibrational parts of the wave function for the asymptotic states. The BO approximation is an excellent approximation for the electronic ground state of the majority of molecules and is assumed here to be valid also for the excited states under consideration.

The differential cross section for the excitation of the vth vibrational level of the αth electronic state is given by (in atomic units, $\hbar = e = m_e = 1$)

$$d\sigma_{v \leftarrow 0}^{\alpha \leftarrow 1}/d\Omega = \left(\frac{\Omega_N}{2\pi} \right)^2 \frac{k_f}{k_i} | \langle f | T | i \rangle |^2 \tag{2.7}$$

with

$$T = V + V(E_t - H_0 + i\eta)^{-1} T = V + V(E_t - H_0 + i\eta)^{-1} V + \cdots , \tag{2.8}$$

where $E_t = E_i + \langle 0 | \tilde{H}_0 | 0 \rangle$ is the total energy and $E_i = k_i^2/2$ is the kinetic energy of the incident electron. η is the usual positive infinitesimal and Ω_N is the normalization volume which drops out of the final expressions. Taking account of equation (2.5) we can integrate over the electronic coordinates in each term arising from the expansion (2.8). The resulting infinite series, which still contains vibrational operators, can be summed exactly, giving

$$\langle f | T | i \rangle = \langle v^{\alpha} | V_{dk_f}^{\alpha *} (E_t - \mathscr{H})^{-1} V_{dk_i}^{1} | 0 \rangle , \tag{2.9a}$$

where

$$\mathscr{H} = \tilde{H}_0 + \epsilon_d + \Delta^t(E_t - \tilde{H}_0) - \frac{i}{2} \Gamma^t(E_t - \tilde{H}_0) , \tag{2.9b}$$

$$\Delta^t(E) = \sum_{\alpha} \Delta^{\alpha}(E) = \sum_{\alpha} (2\pi)^{-1} P \int dE' \frac{\Gamma^{\alpha}(E')}{E - E'} , \tag{2.9c}$$

$$\Gamma^t(E) = \sum_{\alpha} \Gamma^{\alpha}(E) = \sum_{\alpha} 2\pi \sum_{k} V_{dk}^{\alpha} \delta(E - \epsilon_k) V_{kd}^{\alpha} . \tag{2.9d}$$

The non-Hermitian Hamiltonian $\mathscr{H}$ describes the vibrational motion in the resonance state. Here we have introduced the level-shift functions $\Delta^{\alpha}(E)$ and the width functions $\Gamma^{\alpha}(E)$. The partial electronic decay widths of the resonance are given by $\Gamma^{\alpha}(E)$ and the level shift of the localized state is given by $\Delta^t(E)$. The decay widths (Γ^{α}) and level shifts (Δ^{α}) depend not only on the kinetic energy of the scattered electron but also—via $\tilde{H}_0$—on the internuclear distance R and the momentum of nuclear motion. The dependence of the resonance position and width on the nuclear momentum is, by definition, a nonadiabatic effect.

The integral electronic and vibrational excitation functions are

$$\sigma_{v \leftarrow 0}^{\alpha \leftarrow 1}(E) = \frac{\pi \nu}{2E_i} \Gamma^{\alpha}(E_f) \Gamma^1(E_i) | \langle v^{\alpha} | (E_t - \mathscr{H})^{-1} | 0^1 \rangle |^2 . \tag{2.10}$$

Here ν represents the spatial degeneracy of the discrete state. E_f is the final kinetic energy of the electron. Equation (2.10) together with Eqs. 2.9(b)–2.9(d) represent the exact formal solution of the multichannel problem of an electronic resonance coupled to many electronic continua and the vibrational motion.

III. POTENTIAL-ENERGY CURVES, FIXED-NUCLEI CROSS SECTIONS, AND POLES OF THE S MATRIX

In this section we consider the electron-molecule scattering problem in the fixed-nuclei limit. We shall confine ourselves to the two-channel problem for the sake of simplicity. The extension of the formalism to more than two channels is absolutely straightforward.

A. General

In the fixed-nuclei limit, $T_N \to 0$, the operator $E_t - \tilde{H}_0$ appearing in the argument of Γ^t and Δ^t in Eq. (2.9b) reduces to

$$E = E_t - V_0(R) , \tag{3.1}$$

where E_t is the total energy which is conserved in the scattering process and E is the kinetic energy of the incident electron. In the fixed-nuclei limit the integral electronic excitation functions are

$$\sigma^{\alpha \leftarrow 1}(E) = \frac{\pi\nu}{2E}\Gamma^{\alpha}(E - E^{\alpha}_{\rm ex})\Gamma^{1}(E) \times \frac{1}{(E - \epsilon_d - \Delta^t)^2 + (\Gamma^t/2)^2} . \tag{3.2}$$

It is useful to rewrite Eq. (3.2) in terms of the spectral function $A_d(E)$ of the discrete state

$$\sigma^{\alpha \leftarrow 1}(E) = \frac{\pi^2\nu}{E}\frac{\Gamma^{\alpha}(E - E^{\alpha}_{\rm ex})}{\Gamma^t(E)} A_d(E)\Gamma^1(E) , \tag{3.3a}$$

$$\sigma^{\rm tot}(E) = \sum_{\alpha} \sigma^{\alpha \leftarrow 1}(E) , \tag{3.3b}$$

where

$$A_d(E) = \frac{1}{\pi}\frac{\Gamma^t/2}{(E - \epsilon_d - \Delta^t)^2 + (\Gamma^t/2)^2} . \tag{3.3c}$$

Here $\Gamma^1(E)$ and $\Gamma^{\alpha}(E - E^{\alpha}_{\rm ex})$ are the partial widths for entering the resonance from channel 1 and for leaving the resonance into channel α, respectively. Apart from the factors $\Gamma^1(E)$ and the inverse of the kinetic energy of the incident electron, the total integral cross section $\sigma^t(E)$ consists of a number of superimposed spectral functions of the localized state $|d\rangle$, weighted by the *energy-dependent* ratios of the partial decay widths to the total width (Γ^{α}/Γ^t).

In the case of the two-channel problem, the fixed-nuclei T matrix which leads to the cross section (3.3a) can be written as

$$\underline{T}(E) = \frac{1}{E - \epsilon_d - \Delta^t + i\Gamma^t/2}\begin{bmatrix} |V^g_{dk}|^2 & V^{e*}_{dk}V^g_{dk} \\ V^{g*}_{dk}V^e_{dk} & |V^e_{dk}|^2 \end{bmatrix} . \tag{3.4}$$

Here we use g (ground state) and e (excited state) as the electronic channel indices.

A criterion for the occurrence of a resonance in the scattering cross section is an increase of the phase shift by approximately π. The position of the resonance may be defined as the energy where the K matrix has a singularity.[30,31] The real K matrix is given by

$$\underline{K}(E) = -\pi\underline{T}(\underline{1} - i\pi\underline{T})^{-1} = \frac{-\pi}{E - \epsilon_d - \Delta^t}\begin{bmatrix} |V^g_{dk}|^2 & V^{e*}_{dk}V^g_{dk} \\ V^{g*}_{dk}V^e_{dk} & |V^e_{dk}|^2 \end{bmatrix} . \tag{3.5}$$

Obviously, the singularities of the K matrix are given by the solutions of

$$E - \epsilon_d(R) - \Delta^t(E) = 0 . \tag{3.6}$$

When the complex level-shift function $\Delta^t - i\Gamma^t/2$ varies *slowly* in the neighborhood of the resonance, the line shape of the spectral function becomes approximately Lorentzian. An expansion of $\Delta^t - i\Gamma^t/2$ about the solution of Eq. (3.6) yields[32,33]

$$A_d(E) \simeq \frac{Z(E_p)}{\pi}\frac{\Gamma^{\rm eff}/2}{(E - E_p)^2 + (\Gamma^{\rm eff}/2)^2} \tag{3.7}$$

with the effective width

$$\Gamma^{\rm eff} = Z(E_p)\Gamma^t(E_p) \tag{3.8}$$

and

$$Z(E_p) = \left[1 - \frac{\partial}{\partial E}\Delta^t(E)\right]^{-1}\Bigg|_{E=E_p} . \tag{3.9}$$

Here E_p is the solution of Eq. (3.6) and $Z(E_p)$ is the renormalization factor, which is essentially the residue of the pole of the K matrix. It shows how much of the original unperturbed strength remains in the resonance peak at $E = E_p$. Note that the main resonance peak at E_p not only becomes reduced in strength due to $Z(E_p)$, but also in width.

An alternative possibility in looking for resonances is to continue analytically the S matrix into the complex momentum or energy plane and to search for poles of the S matrix.[30,31] For the present problem, the S matrix is given by

$$\underline{S} = \underline{1} - 2\pi i\underline{T} = \frac{1}{E - \epsilon_d - \Delta^t + i\Gamma^t/2}\begin{bmatrix} E - \epsilon_d - \Delta^t + i\pi(|V^e_{dk}|^2 - |V^g_{dk}|^2) & -2\pi i V^{e*}_{dk}V^g_{dk} \\ -2\pi i V^{g*}_{dk}V^e_{dk} & E - \epsilon_d - \Delta^t + i\pi(|V^g_{dk}|^2 - |V^e_{dk}|^2) \end{bmatrix} . \tag{3.10}$$

The poles of the S matrix are given by the solutions of

$$z-\epsilon_d-\Delta^t(z)+\frac{i}{2}\Gamma^t(z)=0\ , \tag{3.11}$$

where z denotes the complex energy variable. It is convenient to introduce the complex channel momentum variables $k_i=u_i+iv_i$ which are related to the complex channel energies z_i via $z_i=(k_i)^2/2$. The channel momentum k_2 is defined by

$$k_2=[(k_1)^2-2E_{\rm ex}]^{1/2}\ . \tag{3.12}$$

In a two-channel problem, the energy plane is a four-sheeted Riemann surface.[30,31] In terms of the channel momenta, the sheets are defined as follows: physical sheet (P),

$$v_1>0,\quad v_2>0\ ; \tag{3.13a}$$

first unphysical sheet (U1),

$$v_1<0,\quad v_2>0\ ; \tag{3.13b}$$

second unphysical sheet (U2),

$$v_1<0,\quad v_2<0\ ; \tag{3.13c}$$

third unphysical sheet (U3),

$$v_1>0,\quad v_2<0\ . \tag{3.13d}$$

In the present case we shall consider the U1 and U2 sheets for the analysis. These are the relevant sheets to describe resonances in the vicinity of the electronic excitation threshold.

To find the poles of the analytically continued S matrix, we define

$$F^e(z_2)=\frac{1}{2\pi}\int dE\frac{\Gamma^e(E)}{z_2-E}\ . \tag{3.14a}$$

We then have for z_2 on the real axis, $z_2=E_2\pm i\eta$,

$$\mathrm{Re}F^e(E_2\pm i\eta)=\Delta^e(E_2)\ , \tag{3.14b}$$

$$\mathrm{Im}F^e(E_2\pm i\eta)=\mp\Gamma^e(E_2)/2\ . \tag{3.14c}$$

$F^e(z_2)$ is thus the analytic continuation of $\Delta^e(E_2)-i\Gamma^e(E_2)/2$ into the upper half of the energy plane. When considered as a function on the complex k_2 plane, $F^e(k_2)$ satisfies the symmetry requirement[30,31]

$$F^e(-k_2^*)=F^e(k_2)^*\ . \tag{3.14d}$$

Analogously defining $F^g(k_1)$, Eq. (3.11) for the poles of the S matrix becomes

$$\tfrac{1}{2}k_2^2+E_{\rm ex}-\epsilon_d(R)-F^e(k_2)-F^g(k_1)=0\ . \tag{3.15}$$

The solutions of Eq. (3.15) are associated with different sheets of the energy plane according to the definition (3.13).

To construct the analytic function $F^{e,g}(k)$ according to Eq. (3.14a), we have to know the energy dependence of the width function $\Gamma^{e,g}(E)$. Being interested in resonances close to the threshold of an electronic channel, we may represent $\Gamma^e(E)$ by its threshold expansion. From the general theory of threshold laws[34,35] we know that the threshold onset of Γ is determined by the centrifugal potential in the absence of other long-range potentials. Introducing a partial-wave representation of the continuum, the width function can be written as

$$\Gamma^e(E')=\sum_{l=0}^{\infty}\Gamma_l^e(E')\ , \tag{3.16}$$

where $E'=E-E_{\rm ex}$ and E is the kinetic energy of the incident electron. The threshold energy dependence of $\Gamma_l(E')$ is given by[34]

$$\Gamma^e(E')\sim(E')^{(2l+1)/2}\ . \tag{3.17}$$

It is thus clear that the lowest angular momentum allowed by the symmetry selection rules dominates the energy dependence of the width at threshold. A simple parametrization of the width function which is in accord with the threshold law is given by[20]

$$\Gamma^e(E')=A(E'/B)^{\alpha}(2-E'/B)^{\alpha}\ , \tag{3.18}$$

where A, B, and α are free parameters. The threshold exponent α is equal to $(2l+1)/2$ in the absence of long-range potentials and takes non-half-integral values in the presence of a (subcritical) dipole potential.[36–41,19] A is the maximum value of the width and $2B$ determines the energy range for which $\Gamma^e(E)$ is different from zero. $\Gamma^e(E')$ has to vanish at high energies to guarantee the existence of the Hilbert transform in Eq. (2.9c). The detailed shape of $\Gamma^e(E')$ at high energies is irrelevant for the scattering near threshold and we choose the simple symmetric form (3.18) for convenience.

Being interested in resonances near the electronic excitation threshold, the form of the decay width associated with the electronic ground state of the target is not of relevance for the results. For simplicity we assume

$$\begin{aligned}&\Gamma^g(E)=\Gamma_0=\text{const}\ ,\\ &\Delta^g(E)=0\end{aligned} \tag{3.19}$$

in the energy region close to the threshold. Throughout the present work we choose $\Gamma_0=0.5$ eV.

B. s-wave scattering from short-range potentials

Putting $\alpha=\frac{1}{2}$ in Eq. (3.18), the width function reads

$$\Gamma^e(E')=A[(E'/B)(2-E'/B)]^{1/2} \tag{3.20}$$

and exhibits the threshold behavior $\Gamma(E')\sim(E')^{1/2}$ appropriate for s-wave scattering. The level-shift function follows from (3.20) with the use of (2.9c):

$$\Delta^e(E')=\tfrac{1}{2}A\{E'/B-1+a[(E'/B)(E'/B-2)]^{1/2}\}\ , \tag{3.21}$$

where $a=1$ for $E'<0$ and $a=0$ for $0<E'<2B$.

We obtain the singularities of the K matrix by solving Eq. (3.6). The dependence of the poles of the K matrix on the internuclear distance R is determined by the energy

$\epsilon_d(R)$ of the discrete state. For the purpose of illustration we take ϵ_d as a linear function of R:

$$\epsilon_d(R)=\epsilon_d(R_0)+\epsilon_d'(R_0)\bar{R}\ , \tag{3.22}$$

where $\bar{R}=R-R_0$. Here R_0 is the equilibrium internuclear distance of the target molecule. For a given internuclear distance R the solutions of Eq. (3.6) are determined by the intersection points of the straight line $E-\epsilon_d(R)$ with the level-shift function $\Delta^t(E)$. The graphical solution of Eq. (3.6) is illustrated in Fig. 1(a). The full curve in Fig. 1(a) represents the level-shift function $\Delta^t(E)$ for $A=1.3$ eV, $B=10$ eV, $E_{ex}=10.78$ eV. Anticipating a later application to a specific problem, we choose for the remaining parameters $\epsilon_d(R_0)=12.68$ eV, $\epsilon_d'(R_0)=-15.76$ eV Å^{-1}. Three typical intersections with $E-\epsilon_d(R)$ are shown in Fig. 1(a).

We now depict the results obtained from the solution of Eq. (3.6) as adiabatic potential-energy curves of resonances by simply plotting the total fixed-nuclei energy

$$E_t=E+V_0(R)\ , \tag{3.23}$$

where $V_0(R)$ is the electronic potential energy of the target and E is the energy relative to $V_0(R)$. The particular form of $V_0(R)$ is not of relevance for the present discussion. The simplest choice is a harmonic potential-energy curve

$$V_0(R)=\tfrac{1}{2}V_0''(R_0)\bar{R}^2\ . \tag{3.24}$$

With ϵ_d given by Eq. (3.22), the potential-energy curve of the discrete state, $V_d(R)=V_0(R)+\epsilon_d(R)$, represents a shifted harmonic oscillator. The potential curves $V_{ex}(R)=V_0(R)+E_{ex}$ (for simplicity E_{ex} is taken to be independent of R) and $V_d(R)$ are shown in Fig. 1(b) as the solid curve and the dashed curve, respectively, where we have chosen $V_0''(R_0)/2=59.72$ eV Å^{-2}. The chain curve represents the singularity of K matrix [the solution of Eq. (3.6)].

The potential curves show that for $\bar{R}\gtrsim 0.07$ Å there exists a solution below the electronic excitation threshold V_{ex}. This solution represents an electronic state of the target-plus-projectile system which is bound with respect

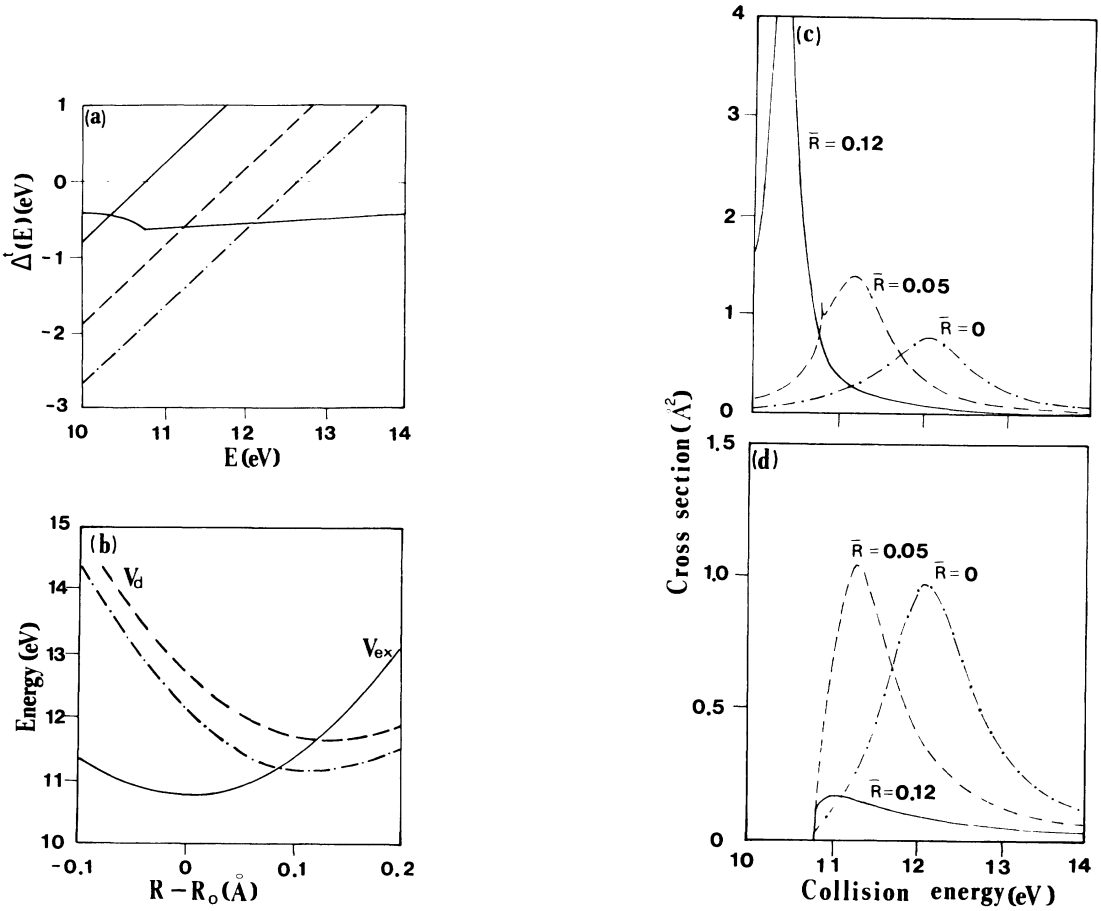

FIG. 1. (a) Graphical determination of the singularity of the K matrix for s-wave scattering. Full curve represents the level-shift function $\Delta^t(E)$. Typical intersections with the straight line $E-\epsilon_d(R)$ are shown. (b) Fixed-nuclei potential-energy curves for s-wave scattering. $V_{ex}(R)$ (solid curve) is the electronic excitation threshold of the target. $V_d(R)$ (broken curve) is the potential-energy curve of the discrete state interacting with the two continua. Chain curve represents the potential curve of the resonance (singularity of the K matrix). (c) Fixed-nuclei electronically elastic cross section for s-wave scattering as a function of energy for three representative values of the internuclear distance. $\bar{R}$ stands for $R-R_0$, where R_0 is the equilibrium distance of the target molecule. (d) Fixed-nuclei electronically inelastic cross section for s-wave scattering as a function of energy for three representative values of the internuclear distance.

to V_{ex}. However, this bound state can decay into the continuum associated with the electronic ground state of the target molecule. This state thus becomes a resonance—a so-called Feshbach resonant state.[2] For $\bar{R} \lesssim 0.07$ Å there is a solution of Eq. (3.6) above the threshold V_{ex}. This state can decay into the continua associated with both the electronic excited *and* the ground state of the target molecule. This state is a so-called core-excited shape resonant state.[2] Note that the two resonances join *continuously* at the threshold.

In Figs. 1(c) and 1(d) we show the fixed-nuclei integral elastic and inelastic cross sections calculated from Eq. (3.2). When the resonance lies below the threshold E_{ex}, the elastic cross section shows a narrow resonance peak. The width of this Feshbach resonance peak is given by $\Gamma_{eff}=Z(E_p)\Gamma_0$, where $Z(E_p)$ is defined in Eq. (3.9). Inspection of Eqs. (3.9) and (3.21) shows that $Z(E_p)$ decreases from approximately unity to zero as the resonance approaches the threshold from below. The Feshbach resonance peak thus becomes narrower as it moves closer to threshold (with decreasing $\bar{R}$). Once the resonance is above the threshold E_{ex}, the width increases because decay in the second channel is now possible. For a resonance immediately at threshold, Eqs. (3.6)—(3.9) are not applicable since Δ^t and Γ^t are rapidly varying functions of energy. Correspondingly, the elastic and inelastic cross sections exhibit a non-Lorentzian profile in this case.

For certain values of the internuclear distance [e.g., $\bar{R}=0.05$ Å, see Fig. 1(c)] the elastic cross section shows a so-called Wigner cusp[31] at the threshold $E=E_{ex}$. This cusp structure is associated with the strong and nearly vertical onset of the inelastic cross section at threshold [see Fig. 1(d)]. The existence of cusp structures reflects the unitarity of the S matrix (3.10). The S matrix of the present resonance model is unitary since we take full account of the energy dependence of the complex level-shift function $\Delta^t-(i/2)\Gamma^t$ near the excitation threshold. Wigner cusps of this type are a well-known phenomenon in electron-He scattering,[1] for example.

As ϵ_d increases further (R decreases), both elastic and inelastic scattering cross sections show a core-excited shape resonance (see Fig. 1). The shape of the resonance peak can be approximated by a Lorentzian profile and the linewidth of the resonance peak can be well approximated by $\Gamma^e(E_p)+\Gamma_0$ where E_p is the position of the core-excited shape resonance.

For a deeper understanding of the cross sections and a proper mathematical description of resonances near excitation thresholds we consider the poles of the S matrix. For s-wave scattering from short-range potentials the function $F^e(z)$ [see Eq. (3.14a)] becomes, in terms of the channel momentum variable k_2,

$$F^e(k_2)=-\frac{A}{4B}[2B-k_2^2+ik_2(4B-k_2^2)^{1/2}] . \quad (3.25)$$

This function is single-valued and analytic in the complex k_2 plane, cut along the real axis from $\pm 2\sqrt{B}$ to infinity. The branch points at $k_2=\pm 2\sqrt{B}$ are a consequence of the artificial cutoff of $\Gamma^e(E')$ at $E'=2B$ and are thus not of physical relevance.[20]

With Eq. (3.19), Eq. (3.15) reduces to

$$\tfrac{1}{2}k_2^2+E_{ex}-\epsilon_d(R)-F^e(k_2)+(i/2)\Gamma_0\mathrm{sgn}(u_1)=0 . \quad (3.26)$$

As we are particularly interested in the vicinity of the threshold, u_1 is large and will not change sign within the range of the values of k_2 of interest. We may take the sign of u_1 as positive. Figure 2 shows the resulting trajectories of the poles of the S matrix in the complex k_2 plane in the vicinity of the origin, obtained as the solution of Eq. (3.26). For comparison we show also the trajectories of the poles of the S matrix in the limit of vanishing Γ_0 (i.e., the one-channel case) by the dashed lines.

In the single-channel case ($\Gamma_0=0$) there are two resonance poles of the S matrix in the lower half of the k_2 plane, situated *symmetrically* to the imaginary axis. With increasing R the poles move inward essentially parallel to the real axis and meet on the negative imaginary axis, where a pair of virtual states is created. With further increasing $\bar{R}$ one virtual-state pole moves down the imaginary axis, while the other moves upwards and crosses the origin to become a bound-state pole. These pole trajectories are in full accord with the general results of analytic S-matrix theory for single-channel s-wave scattering.[30,31]

When Γ_0 is nonzero there are, for each internuclear distance $\bar{R}$, two resonance poles, in the right and left halves of the k_2 plane. In contrast to the single-channel case, they are situated *nonsymmetrically* to the imaginary axis. The resonance pole in the fourth quadrant moves inward with increasing $\bar{R}$ and further away from the real axis. It approaches the negative imaginary axis for $\bar{R}\to\infty$. The resonance pole in the left half-plane moves from the third quadrant into the second quadrant as $\bar{R}$ increases. It approaches the positive imaginary axis for $\bar{R}\to\infty$.

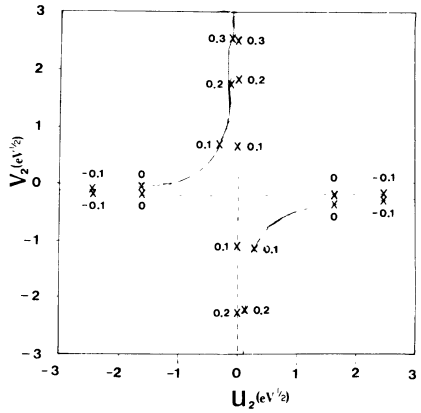

FIG. 2. Trajectories of the poles of the fixed-nuclei S matrix for s-wave scattering in the complex *momentum* plane. Numbers give the corresponding internuclear distance $\bar{R}$ (in Å) to indicate the movement of poles with $\bar{R}$. Broken lines indicate the trajectories of the poles in the case of $\Gamma_0=0$ (single-channel case).

When the k_2 plane is mapped on to the complex energy plane $z_1 = x_1 + iy_1$ via $z_1 = k_2^2/2 + E_{ex}$, we obtain Fig. 3. The energy plane shown is actually a two-sheeted Riemann surface. The first unphysical (U1) sheet corresponds to the upper half of the k_2 plane, the second unphysical (U2) sheet to the lower half of the k_2 plane. For comparison we show the trajectories of the poles of the S matrix in the limit of vanishing Γ_0 by the dashed lines. In the case of $\Gamma_0 = 0$, poles on the physical sheet ($v_2 > 0$) are indicated by circles, poles on the unphysical sheet ($v_2 < 0$) by crosses. The resonance poles on the unphysical sheet are situated symmetrically to the real axis and move towards the axis with increasing $\bar{R}$. They meet on the real axis slightly below the threshold E_{ex}. Then one pole moves down the real axis and the other upwards, both being on the unphysical sheet. The latter pole moves onto the physical sheet at the threshold and then moves down the real axis on the physical sheet.

When Γ_0 is nonzero, we obtain the trajectories given by the full lines in Fig. 3. The lower trajectory on the U2 sheet (Fig. 3) corresponds to the resonance pole in the second quadrant of the k_2 plane. The resonance pole in the upper half of the U2 plane corresponds to the resonance pole in the third quadrant of the k_2 plane. With increasing R the resonance pole moves from the U2 sheet onto the U1 sheet (i.e., y_1 goes through zero). The pole on the U1 sheet is indicated by circles in Fig. 3. Note that the two Feshbach resonance poles below the threshold E_{ex} are on different Riemann sheets. The pole trajectories shown in Figs. 2 and 3 are a general result for multichannel s-wave scattering in the absence of long-range potentials.

The comparison of the present results with the case of the one-channel problem ($\Gamma_0 = 0$) shows that the trajectories of the poles in the energy plane are shifted downward by $\Gamma_0/2$ in the asymptotic limit $\bar{R} = \pm\infty$. For large $\bar{R}$ the Feshbach resonance pole on the U2 sheet describes the sharp resonance peak in the elastic cross section below threshold [see Fig. 1(c)]. For small $\bar{R}$, the core-excited shape resonance pole in lower half U2 sheet describes the "broad" resonance structure above threshold in the elastic and inelastic cross sections [see Figs. 1(c) and 1(d)]. However, the above-mentioned non-Lorentzian profile for a resonance very close to threshold cannot be described by the complex poles of the S matrix.

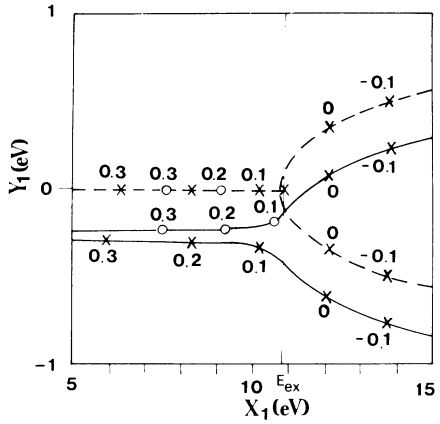

FIG. 3. Trajectories of the poles of the fixed-nuclei S matrix for s-wave scattering in the complex *energy* plane. Numbers give the corresponding internuclear distance $\bar{R}$ (in Å) to indicate the movement of poles with $\bar{R}$. Broken lines indicate the trajectories of the poles in the case of $\Gamma_0 = 0$. Circles indicate poles on the first unphysical (U1) sheet, the crosses poles on the second unphysical (U2) sheet.

The behavior of the poles of the S matrix near the excitation threshold illustrated in Figs. 2 and 3 is known as the "shadow pole" phenomenon. It has been discussed in a different context (classification of meson-baryon resonances by symmetry schemes which are partially violated) in Refs. 42–44. It can be shown under rather general assumptions about unitarity and analyticity that the existence of a resonance pole of the multichannel S matrix requires the existence of shadow poles on other Riemann sheets in the energy variable.[44] In particular, the trajectories of the poles representing the resonance above threshold (in the fourth quadrant of the k_2 plane) and the resonance below threshold (in the second quadrant) are *not* connected (see Fig. 2). This is in contrast to the single-channel case, where the resonance pole trajectory is connected with the bound-state pole trajectory (via a virtual-state pole trajectory). A model similar to the present one has been discussed by Ross[42] for the case $l = 1$, i.e., p-wave scattering.

It is straightforward to extend the present analysis to scattering in partial waves $l > 0$ as outlined in the single-channel case in Ref. 20. For $l > 0$, $\Gamma^e(E)$ and $\Delta^e(E)$ are smooth functions of energy at the threshold E_{ex}. Therefore, deviations from the Lorentzian line shape are weak and threshold effects such as Wigner cusps are absent.

C. Scattering from polar molecules

It is well known that long-range potentials are of crucial importance in electron-atom or electron-molecule scattering near threshold.[36–38,40] In particular, resonances near threshold are affected by the modification of the threshold onset of the width function $\Gamma(E)$.[19] In this section we present an example of the impact of a long-range potential on a resonance near an electronic excitation threshold. We consider a discrete state coupled to a continuum distorted by a critical dipole potential. A critical dipole ($D_c = 1.625$ debye) is a dipole which is just not strong enough to bind an electron. In the presence of a dipole potential, the threshold exponent of the width function (3.18) is a real number α with $0 < \alpha < \frac{1}{2}$. Here, $\alpha = \frac{1}{2}$ corresponds to a vanishing dipole moment of the target molecule, $\alpha = 0$ to the critical dipole moment.[36–38]

Putting $\alpha = 0$ in Eq. (3.18) the width function reads

$$\Gamma^e(E') = \begin{cases} A, & \text{for } 0 < E' < 2B \\ 0, & \text{elsewhere} . \end{cases} \tag{3.27}$$

Thus the square-root onset of $\Gamma^e(E')$ in the case of pure s-wave scattering is converted into a step-function onset

when the dipole moment approaches the critical value. The level-shift function reads

$$\Delta^e(E') = \frac{A}{2\pi} \ln \left| \frac{E'}{2B - E'} \right| . \tag{3.28}$$

The level-shift function is shown as the full curve in Fig. 4(a). As in Sec. III B, we take $A = 1.3$ eV, $B = 10.0$ eV, $\epsilon_d'(R_0) = -15.76$ eV Å^{-1}, and $\Gamma_0 = 0.5$ eV. Four typical intersections with the straight line $E - \epsilon_d(R)$ are shown in Fig. 4(a) to illustrate the graphical determination of the singularities of the K matrix [Eq. (3.6)]. The level-shift function possesses a logarithmic singularity at threshold. As a consequence we find three intersection points of $\Delta^t(E)$ with the straight line $E - \epsilon_d(R)$ when $\epsilon_d(R)$ exceeds some critical value $\epsilon_d^c(R)$ ($= 11.9$ eV), in contrast to the case of pure s-wave scattering where a *single* solution of Eq. (3.6) is obtained for each R. One of these intersection points occurs below threshold and the other two intersection points are above threshold. When $\epsilon_d(R)$ is below the critical value, only one intersection point is obtained below threshold.

Figure 4(b) shows the resulting fixed-nuclei potential-energy curves. The parameters used are the same as in Fig. 1(b). The dashed-dotted curve representing a singularity of the K matrix does not simply cross the threshold, as it does in the absence of long-range potentials. The potential-energy curve of the resonance solution of Eq. (3.6) "bends back" when approaching the threshold and runs parallel and extremely close to the threshold for $\bar{R} \lesssim 0$ Å. The solution below threshold exists over the whole range of internuclear distances and lies extremely close to the threshold for $\bar{R} \lesssim 0$ Å. This unusual behavior of the potential-energy curves is easily understood from the

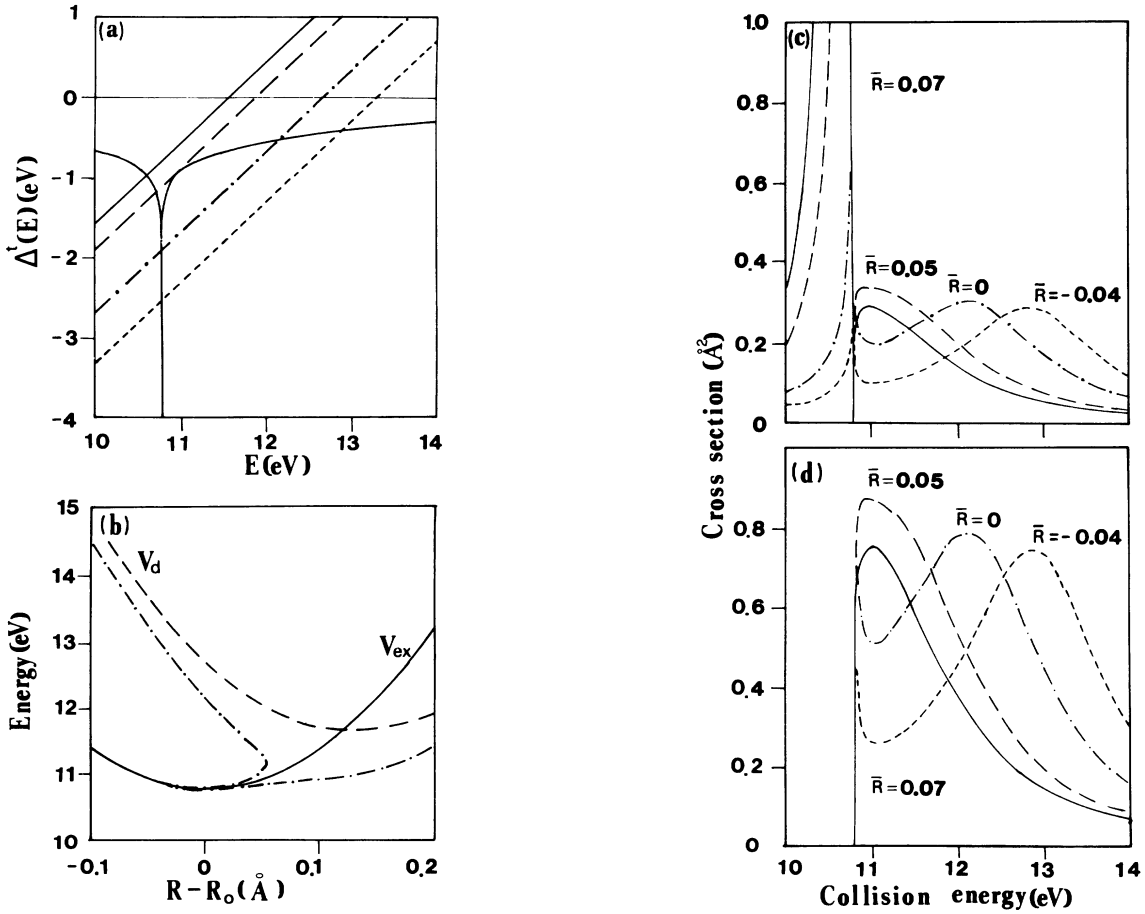

FIG. 4. (a) Graphical determination of the singularities of the K matrix for electron-polar molecule scattering. Full curve represents the level-shift function $\Delta^t(E)$ assuming a critical dipole moment. Four typical intersections with the straight line $E - \epsilon_d(R)$ are shown. It is seen that a triple of solutions of Eq. (3.6) exists if $\epsilon_d(R)$ exceeds some critical value. (b) Fixed-nuclei potential-energy curves for a critical dipole moment. $V_{ex}(R)$ (solid curve) is the electronic excitation threshold of the target, $V_d(R)$ (broken curve) the potential-energy curve of the discrete state interacting with the two continua. Chain curves represent the resonances, i.e., the singularities of the K matrix. (c) Fixed-nuclei electronically elastic cross section for a critical dipole moment as a function of energy for four representative values of the internuclear distance. $\bar{R}$ stands for $R - R_0$, where R_0 is the equilibrium distance of the target molecule. (d) Fixed-nuclei electronically inelastic cross section for a critical dipole moment as a function of energy for four representative values of the internuclear distance.

graphical solution of Eq. (3.6) and is a consequence of a long-range dipole potential.[19]

In Figs. 4(c) and 4(d) we show the elastic and inelastic cross sections calculated from Eq. (3.2). Note that the shape of the elastic and inelastic cross sections are identical for $E > E_{ex}$. They are almost identical with that of the spectral function of the localized state because of the present simplified choice of the width functions (step function for Γ^e, constant for Γ^g).

In the elastic scattering cross section there is a very sharp and intense peak just below threshold. This peak is due to the solution of Eq. (3.6) below threshold which always exists. The width of this peak becomes narrower as ϵ_d increases ($\bar{R}$ decreases). For $\epsilon_d \lesssim E_{ex}$ this peak corresponds to a Feshbach resonance state coupled to the electronic ground state of the target molecule by the decay width $\Gamma^{\text{eff}} = Z(E_p)\Gamma_0 \simeq \Gamma_0$.

For $\epsilon_d \gtrsim E_{ex}$, this Feshbach resonance state is now a state "split off" from the bottom of the continuum due to mixing of the localized discrete state with the continuum. Physically, this is a state supported mainly by the dipole potential.[19,20] For $\epsilon_d \gtrsim E_{ex}$, $Z(E_p)$ becomes much smaller than 1 and approaches zero. The width of the Feshbach resonance peak is then $\Gamma^{\text{eff}} = Z(E_p)\Gamma_0 \ll \Gamma_0$ [see Eq. (3.8)], i.e., the Feshbach resonance becomes extremely narrow [see Fig. 4(d)]. Note that the renormalization factor $Z(E_p)$ becomes much smaller here than in the case of pure s-wave scattering discussed in Sec. III B, where $Z(E_p) \to 0$ only in a very narrow energy interval just below threshold.

For $\bar{R} \lesssim 0$ we observe a sharp threshold peak in the inelastic cross section which becomes smaller as ϵ_d increases. This is certainly a new feature which is not observed in the inelastic cross section for s-wave scattering in the absence of long-range potentials. This peak reflects the presence of a Feshbach resonance state supported by a dipole potential just below threshold. This peak is thus interpreted as a dipole-moment-induced threshold effect.

The other structure at higher energy is a "broad" resonance structure which represents a core-excited shape resonance for large ϵ_d (small $\bar{R}$) as in the case of pure s-wave scattering. This core-excited shape resonance can be approximated by a Lorentzian like spectral function and the width can be approximated by $\Gamma^e + \Gamma_0$. In contrast to the case of pure s-wave scattering discussed in Sec. III.B a core-excited shape resonance above threshold exists *together* with a Feshbach resonance below threshold for a range of internuclear distances.

For a further understanding of the cross sections and a more precise mathematical description of resonances, we now look for poles of the analytically continued S matrix. When $\Gamma^e(E)$ is given by the step function of Eq. (3.27), we obtain from Eq. (3.14a)

$$F^e(k_2) = \frac{A}{2\pi} \ln \frac{k_2^2}{k_2^2 - C^2} , \tag{3.29}$$

where

$$C^2 = 4B .$$

$F^e(k_2)$ has branch points at $k_2 = \pm C$ and at $k_2 = 0$. To obtain a single-valued function we have to cut the k_2 plane along the real axis for $|k_2| > C$ and along the negative imaginary axis. The branch lines on the real axis are a consequence of the unphysical cutting off of $\Gamma^e(E')$ at $E' = 2B$ in Eq. (3.27) and thus of no physical significance.[19] The branch cut on the negative imaginary axis, on the other hand, is a consequence of the steplike onset of $\Gamma^e(E')$ at threshold and reflects the effect of the long-range dipole potential. The symmetry of $F^e(k_2)$ [Eq. (3.14d)] implies that $F^e(k_2)$ has to be real on the positive imaginary axis, i.e., the argument of the logarithm is defined as zero on the positive imaginary axis.

Figure 5 shows the resulting trajectories of the poles of the S matrix in the complex k_2 plane, obtained as the solutions of Eq. (3.26). For illustrative purposes, the trajectories of the poles of the S matrix in the limit of vanishing Γ_0 (single-channel case) are also shown as dashed lines. For $\Gamma_0 = 0$ we have, for each internuclear distance R, a bound-state pole on the positive imaginary axis as well as two resonance poles in the lower half-plane, situated symmetrically to the imaginary axis. The bound-state pole starts at the origin for $\bar{R} = -\infty$ and moves up the positive imaginary axis with increasing $\bar{R}$. The two resonance poles below the real axis move inward with increasing $\bar{R}$ and further away from the real axis. The nonvanishing imaginary part of $F(k_2)$ on the negative imaginary axis prevents them from reaching the axis, i.e., there exist no virtual-state poles in this case.[19,20]

When Γ_0 is nonzero we have, for each internuclear distance $\bar{R}$, three resonance poles. There is no resonance pole in the first quadrant. In the second quadrant of the k_2 plane, a Feshbach resonance pole starts at the origin (for

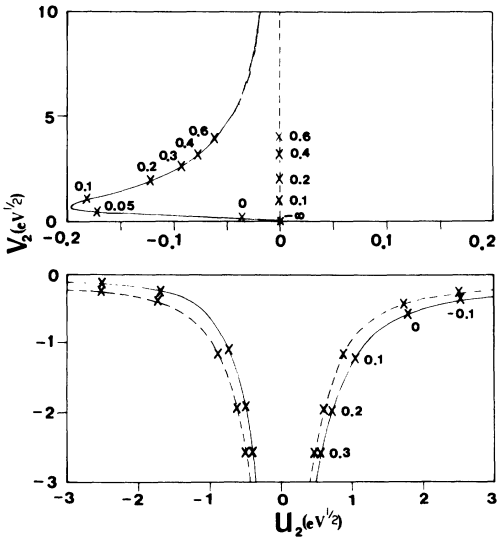

FIG. 5. Trajectories of the poles of the fixed-nuclei S matrix for a critical dipole moment in the complex *momentum* plane. Numbers give the values of the corresponding internuclear distance $\bar{R}$ to indicate the movement of the poles with $\bar{R}$. Trajectories obtained for $\Gamma_0 = 0$ (single-channel case) are given as dashed lines.

$\bar{R}=-\infty$) and moves into the second quadrant at a certain angle given by (for $B \gg 0$)

$$\phi_{uv}=\frac{\pi\Gamma_0}{2A} . \tag{3.30}$$

Here ϕ_{uv} is measured counterclockwise from the positive imaginary axis. Note that the angle is determined by the ratios of the partial decay widths. With increasing $\bar{R}$, the pole trajectory bends back and approaches the positive imaginary axis.

The two resonance poles in the lower half-plane are situated *nonsymmetrically* to the imaginary axis. The term $i\Gamma_0/2$ in Eq. (3.26) displaces the poles nonsymmetrically. The resonance poles move inward with increasing $\bar{R}$ and, at the same time, further away from the real axis. For $\bar{R}\to\infty$ they approach the negative imaginary axis.

When the k_2 plane is mapped onto the U1 and U2 sheets of the complex energy plane $z_1=x_1+iy_1$ via $z_1=k_2^2/2+E_{ex}$, we obtain Fig. 6. For comparison, we show the trajectories of the poles of the S matrix in the single-channel case by the dashed lines.

In the limit of vanishing Γ_0 there is, for each $\bar{R}$, a bound-state pole of the S matrix on the negative real axis of the U1 sheet as well as two resonance poles on the U2 sheet, situated symmetrically to the real axis. The bound-state pole starts at the origin for $\bar{R}=-\infty$ and moves down the negative energy axis with increasing $\bar{R}$. The resonance poles move from right to left with increasing $\bar{R}$ and, at the same time, recede from the real axis.

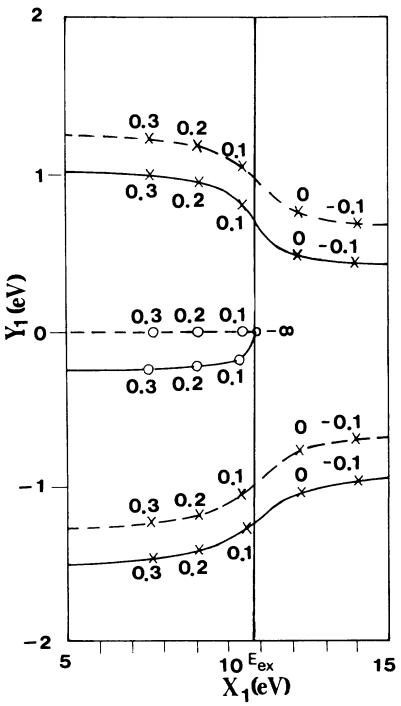

FIG. 6. Trajectories of the poles of the fixed-nuclei S matrix for a critical dipole moment in the complex *energy* plane. Circles indicate poles on the U1 sheet, the crosses poles on the U2 sheet. Trajectories obtained for $\Gamma_0=0$ are given as dashed lines.

In the case of nonzero Γ_0, the resonance pole in the upper half of the k_2 plane is mapped on the U1 sheet and is indicated by circles. The resonance poles in the lower half of the k_2 plane are mapped on the U2 sheet and are indicated by crosses. The Feshbach resonance pole on the lower U1 sheet starts at the origin for $\bar{R}=-\infty$ and leaves the origin at a certain angle given by

$$\phi_{xy}=\frac{\pi\Gamma_0}{A} . \tag{3.31}$$

Here ϕ_{xy} is measured in the counterclockwise sense from the negative real axis. Asymptotically, the imaginary part of the pole position approaches $-\Gamma_0/2$. In the limit $\bar{R}=+\infty$ the trajectories of the poles are displaced by $-\Gamma_0/2$ from the ones obtained for $\Gamma_0=0$. Note that the imaginary part of the pole position decreases very rapidly with $\bar{R}$ in the region $\bar{R}\lesssim 0.1$ Å.

This reflects the pronounced narrowing of the Feshbach resonance peak below threshold in the elastic cross section with decreasing $\bar{R}$ [see Fig. 3(d)]. The resonance pole in the lower half of the U2 sheet describes the core-excited shape resonance in the elastic and inelastic cross sections for small $\bar{R}$ (see Fig. 3). We see explicitly in Fig. 6 that the width is $\Gamma\simeq\Gamma_0+\Gamma^e$. The resonance pole in the upper half of the U2 sheet is physically irrelevant.

The above analysis of the poles of the S matrix gives an analytic description of core-excited shape and Feshbach resonances near threshold of electronic channels with a strong dipole moment. In this description, the Feshbach resonance state emerges naturally as a bound state supported mainly by the dipole potential with a finite width for decay into lower-lying electronic channels. We have seen that the width of this Feshbach resonance may be much smaller than the zeroth-order width Γ_0 which describes the coupling of the discrete state to the lower-lying continuum.

The present study should be considered merely as an illustration of the impact of long-range potentials in electron-molecule scattering near electronic excitation thresholds. As discussed in Sec. IV, the model might be suitable to describe near-threshold electron impact excitation of certain Rydberg states of the CO molecule. However, strong long-range potentials are probably a very common phenomenon in electron scattering from atoms and molecules in electronically excited states, even for symmetric molecules such as N_2 where a permanent dipole moment is forbidden by symmetry. The well-known isotropic dipole potential in electron scattering from the excited H atom[36,37] is probably only the simplest example of correlation-induced long-range potentials.

IV. DYNAMICAL CALCULATIONS OF CROSS SECTIONS

In the preceding sections resonances and threshold effects in electronically inelastic and elastic electron-molecule scattering have been analyzed in the fixed-nuclei limit. General results have been obtained which are of relevance for the interpretation of experimental data.

We have seen in Sec. II that the electronic and vibrational motions are entangled in a complicated way since the complex level-shift function depends not only on the electronic energy E, but also—via $\tilde{H}_0$—on the momenta of the nuclei—a nonadiabatic effect. This nonadiabatic effect will be especially important near threshold where the complex level-shift function varies rapidly.

When the vibrational Hamiltonians $\tilde{H}_0$ and $\tilde{H}_d$ $[=\tilde{H}_0+\epsilon_d(R)]$ of the target state and the discrete state are harmonic oscillators, Eq. (2.10) can be simply evaluated.[45] The effective Hamiltonian $\mathscr{H}$ of (2.9b) is then tridiagonal in the representation of the target vibrational states which leads to a continued-fraction expression for the matrix elements of the resolvent operator $(E_t-\mathscr{H})^{-1}$ in Eq. (2.10). For more details, see Ref. 45.

For s-wave scattering in the absence of long-range potentials we have calculated the $v=0\rightarrow 0$ and $v=0\rightarrow 1$ integral vibrational excitation functions for the parameter values introduced before. The resulting integral vibrational excitation functions are rather similar to the fixed-nuclei cross sections calculated for $\bar{R}=0$ in Sec. III B. There are no dramatic dynamical effects, and we omit a detailed discussion of these results for the sake of brevity.

More interesting is the dipole potential case, discussed in Sec. III C in the fixed-nuclei limit. We have calculated the $0\rightarrow v$ integral vibrational excitation functions for the parameter values introduced before, i.e., $\epsilon_d(R_0)=12.68$ eV, $\epsilon_d'(R_0)=-15.76$ eV Å^{-1}, $V_0''(R_0)=119.4$ eV Å^{-2}, $A=1.3$ eV, $B=10$ eV, and $\Gamma_0=0.5$ eV. Taking $\mu=6.86$ amu, which corresponds to the CO molecule, we obtain $\omega=0.27$ eV and $\kappa=-0.53$ eV for the vibrational frequency and the vibrational coupling constant,[45] respectively. The resulting electronically elastic integral vibrational excitation functions show a very sharp Feshbach resonance peak below threshold as in the fixed-nuclei elastic cross section for $\bar{R}=0$ Å in Fig. 4(d). Due to our assumption of parallel thresholds, the potential-energy curve of the Feshbach resonance is also approximately parallel to the potential-energy curve of the target state. According to the Franck-Condon principle, we observe only the $v=0$ level of the Feshbach resonance in the $0\rightarrow 0$ cross section. In the vibrationally inelastic cross sections $(0\rightarrow v)$ the intensity of the Feshbach resonance peak is strongly reduced due to unfavorable Franck-Condon factors.

In Figs. 7(a) and 7(b) we show the electronically inelastic $v=0\rightarrow 0$ and $v=0\rightarrow 1$ integral cross sections. Note that the shape of the electronically elastic and inelastic $v=0\rightarrow 0$ (and 1) integral vibrational excitation functions are identical above threshold in the present model. For comparison we show in Fig. 7(c) the electronically inelastic cross section in the fixed-nuclei limit (for $\bar{R}=0$). The threshold peak already discussed in Sec. III C is more clearly visible here than in Fig. 4(c). It is seen that the $0\rightarrow 0$ dynamical cross section is similar in shape to the fixed-nuclei cross section, except for the appearance of additional fine structures. The fine structures can be associated with vibrational levels of the Feshbach resonance below the electronic excitation threshold. These levels are embedded in the shape-resonant continuum above the excitation threshold and interact with this continuum via nonadiabatic couplings, leading to narrow resonances with typical Fano line shapes. In the $v=0\rightarrow 1$ excitation function, the threshold peak is reduced in height, whereas the relative intensity of the fine-structure resonances has increased compared to the $v=0\rightarrow 0$ excitation function.

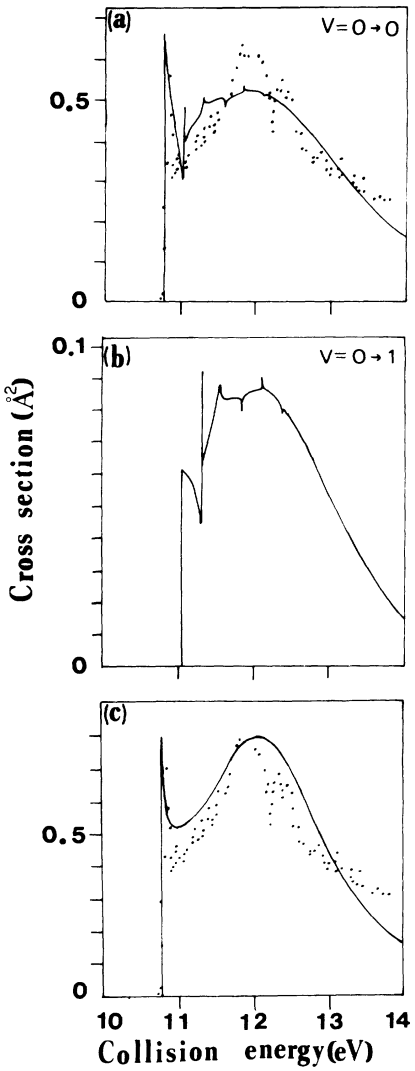

FIG. 7. Electronically inelastic dynamical (a) $v=0\rightarrow 0$ and (b) $v=0\rightarrow 1$ vibrational excitation cross sections corresponding to the fixed-nuclei potential-energy curves of Fig. 4(b) (critical dipole moment). Fixed-nuclei inelastic integral cross section for $\bar{R}=0$ is shown in (c). Dots are experimental data of Mazeau *et al.*[23] for the $v=0\rightarrow 0$ excitation function, measured at a scattering angle of 40°. Experimental data are scaled by an arbitrary factor.

Threshold peaks of the type shown in Fig. 7 have been observed experimentally in the electronic excitation functions of various diatomic molecules.[23,46,47] We have chosen the parameters of our model such as to reproduce qualitatively the measured differential (scattering angle 40°) $v=0\rightarrow 0$ excitation function of the $B\,^1\Sigma^+$ $(5\sigma\rightarrow 3s)$ Rydberg state of the CO molecule.[23] The experimental data are included as dots in Figs. 7(a) and 7(c). Since the

measured cross section is in arbitrary units,[23] we have rescaled the experimental data arbitrarily. The most prominent feature of the experimental data is a sharp threshold peak at 10.78 eV. In addition, a broad resonance near 12 eV, superimposed by sharp fine-structure features is observed. Qualitatively, these features are well reproduced by the present calculation. As shown in Fig. 7(c), the main features of the experiment can already be explained in the fixed-nuclei limit.

The potential-energy curve of the $B\,^1\Sigma^+$ state of CO is nearly parallel with that of the $X\,^1\Sigma^+$ state.[48] Therefore, our assumption of parallel thresholds is reasonable for the problem at hand. The dipole moment of the CO molecule in the $B\,^1\Sigma^+$ state is probably not known. However, recent calculations of dipole moments of excited states of CO predict large dipole moments for the states considered.[49] Moreover, the $X\,^2\Sigma^+$ state of CO^+ has a large dipole moment,[50] which indicates that Rydberg states associated with the $X\,^2\Sigma^+$ core should have significant dipole moments. Therefore, our assumption of a critical dipole moment ($D=1.625$ debye) for the $B\,^1\Sigma^+$ state appears qualitatively reasonable.

Due to the simplifications introduced into the present model [harmonic potential-energy curves for V_0, V_d, and V_{ex}, step function for $\Gamma^e(E)$] one cannot expect that detailed agreement between theory and experiment can be obtained. However, most of the prominent features of the experimental cross sections are qualitatively reproduced by the present calculation. We interpret the sharp peak at threshold as a dipole-moment-induced threshold effect. This peak is due to the presence of a Feshbach resonance state just below threshold, supported by the dipole potential. The maximum on the higher-energy side is interpreted as a core-excited shape resonance. The present dynamical calculations explain the fine structures in the cross section near threshold qualitatively in terms of vibrational levels of a Feshbach resonance embedded in the shape-resonant continuum. However, the present calculation cannot explain all fine structures, especially the dips on the higher-energy side of the shape resonance. These may be attributed to Feshbach resonances associated with higher excited states, e.g., the $C\,^1\Sigma^+$ ($5\sigma\rightarrow 3p\sigma$) state (threshold at 11.4 eV).

Further experimental studies of electronically elastic and inelastic scattering from molecules are necessary to gain a deeper understanding of Feshbach resonances and the associated vibrational levels. The present calculations are of model character due to the oversimplified form of the width function $\Gamma(E)$ and the harmonic approximation for the potential-energy curves of CO and the discrete state of CO^-. With the inclusion of more electronic channels, more accurate potential-energy curves, and realistic width functions, a quantitative description of the experiment should be possible. Further experimental and theoretical studies of the long-range potentials in electron scattering from electronically excited target molecules are necessary to identify the correct threshold behavior of the width functions.

ACKNOWLEDGMENTS

The authors are indebted to L.S. Cederbaum for stimulating discussions. One of the authors (M.O.) would like to express his gratitude to the Alexander von Humboldt Foundation for financial support.

*Present address: Institute of Theoretical Physics, Chalmers University of Technology, S-412 96 Göteborg, Sweden.

[1]G. J. Schulz, Rev. Mod. Phys. 45, 378 (1973).
[2]G. J. Schulz, Rev. Mod. Phys. 45, 423 (1973).
[3]J. N. Bardsley, A. Herzenberg, and F. Mandl, Proc. Phys. Soc. London. 89, 321 (1966).
[4]T. F. O'Malley, Phys. Rev. 150, 14 (1966).
[5]J. N. Bardsley and F. Mandl, Rep. Prog. Phys. 31, 471 (1968).
[6]D. T. Birtwistle and A. Herzenberg, J. Phys. B 4, 53 (1971).
[7]N. Chandra and A. Temkin, Phys. Rev. A 13, 188 (1976).
[8]R. K. Nesbet, Phys. Rev. A 19, 551 (1979).
[9]L. Dubé and A. Herzenberg, Phys. Rev. A 20, 194 (1979).
[10]B. I. Schneider, M. Le Dourneuf, and Vo Ky Lan, Phys. Rev. Lett. 43, 1926 (1979).
[11]A. U. Hazi, T. N. Rescigno, and M. Kurilla, Phys. Rev. A 23, 1089 (1981).
[12]M. Berman, H. Estrada, L. S. Cederbaum, and W. Domcke, Phys. Rev. A 28, 1363 (1983)
[13]K. Rohr and F. Linder, J. Phys. B 9, 2521 (1975).
[14]K. Rohr, J. Phys. B 11, 1849 (1978).
[15]H. S. Taylor, E. Goldstein, and G. A. Segal, J. Phys. B 10, 2253 (1977).
[16]L. Dubé and A. Herzenberg, Phys. Rev. Lett. 38, 820 (1977).
[17]W. Domcke, L. S. Cederbaum, and F. Kaspar, J. Phys. B 12, L359 (1979).
[18]M. R. H. Rudge, J. Phys. B 13, 1269 (1980).
[19]W. Domcke and L. S. Cederbaum, J. Phys. B 14, 149 (1981).
[20]W. Domcke, J. Phys. B 14, 4889 (1981).
[21]H. Feshbach, Ann. Phys. (N.Y.) 5, 357 (1958); Ann. Phys. (N.Y.) 19, 287 (1962).
[22]U. Fano, Phys. Rev. 124, 1866 (1961).
[23]J. Mazeau, F. Gresteau, G. Joyez, J. Reinhardt, and R. I. Hall, J. Phys. B 5, 1890 (1972).
[24]P. A. M. Dirac, Z. Phys. 44, 585 (1927).
[25]V. Weisskopf, Ann. Phys. (Leipzig) 9, 23 (1931).
[26]P. W. Anderson, Phys. Rev. 124, 41 (1961).
[27]J. C. Y. Chen, Phys. Rev. 148, 66 (1966).
[28]J. N. Bardsley, J. Phys. B 1, 349 (1968); 1, 365 (1968).
[29]W. Domcke and L. S. Cederbaum, Phys. Rev. A 16, 1465 (1977).
[30]J. R. Taylor, *Scattering Theory* (Wiley, New York, 1972).
[31]R. G. Newton, *Scattering Theory of Waves and Particles*, 2nd ed. (Springer, Berlin, 1982).
[32]P. Nozières, *Theory of Interacting Fermi Systems* (Benjamin, New York, 1964).
[33]G. E. Brown, *Many-Body Problems* (North-Holland, Amster-

dam, 1972).
[34]E. P. Wigner, Phys. Rev. 73, 1002 (1948).
[35]Reference 31, Sec. 17.2
[36]M. J. Seaton, Proc. Phys. Soc. London 77, 174 (1961).
[37]M. Gailitis and R. Damburg, Proc. Phys. Soc. London 82, 192 (1963).
[38]T. F. O'Malley, Phys. Rev. 137, A1668 (1965).
[39]H. Hotop, T. A. Patterson, and W. C. Lineberger, J. Chem. Phys. 60, 1806 (1974).
[40]I. I. Fabrikant, Zh. Eksp. Teor. Fiz. 73, 1317 (1977) [Sov. Phys.—JETP 46, 693 (1978)].
[41]P. C. Engelking, Phys. Rev. A 26, 740 (1982).
[42]M. Ross, Phys. Rev. Lett. 11, 450 (1963).
[43]M. Nauenberg and J. C. Nearing, Phys. Rev. Lett. 12, 63 (1964).
[44]R. J. Eden and J. R. Taylor, Phys. Rev. 133, B1575 (1964).
[45]W. Domcke and L. S. Cederbaum, J. Phys. B 13, 2829 (1980).
[46]J. Mazeau, F. Gresteau, R. I. Hall, G. Joyez, and J. Reinhardt, J. Phys. B 6, 862 (1973); 6, 873 (1973).
[47]N. Böse and F. Linder, J. Phys. B 12, 3805 (1979).
[48]D. M. Cooper and S. R. Langhoff, J. Chem. Phys. 74, 1200 (1981).
[49]D. Lynch, M. F. Herman, and D. L. Yeager, Chem. Phys. 64, 69 (1982), and references therein.
[50]P. Rosmus and L.-J. Werner, Mol. Phys. 47, 661 (1982).